GA–A24872

ACTIVE MEASUREMENT OF RESISTIVE WALL MODE STABILITY IN ROTATING HIGH BETA PLASMAS

by
H. REIMERDES, J. BIALEK, M.S. CHANCE, M.S. CHU, A.M. GAROFALO,
P. GOHIL, G.L. JACKSON, R.J. JAYAKUMAR, T.H. JENSEN, R.J. LA HAYE,
Y.Q. LIU, J.E. MENARD, G.A. NAVRATIL, M. OKABAYASHI,
J.T. SCOVILLE, E.J. STRAIT, and H. TAKAHASHI

OCTOBER 2004

DISCLAIMER

GA–A24872

ACTIVE MEASUREMENT OF RESISTIVE WALL MODE STABILITY IN ROTATING HIGH BETA PLASMAS

by
H. REIMERDES,* J. BIALEK,* M.S. CHANCE,† M.S. CHU, A.M. GAROFALO,*
P. GOHIL, G.L. JACKSON, R.J. JAYAKUMAR,‡ T.H. JENSEN, R.J. LA HAYE,
Y.Q. LIU,Δ J.E. MENARD,† G.A. NAVRATIL,* M. OKABAYASHI,†
J.T. SCOVILLE, E.J. STRAIT, and H. TAKAHASHI†

This is a preprint of a paper to be presented at the 20th IAEA Fusion Energy Conference, Vilamoura, Portugal, November 1–6, 2004 and to be published in the *Proceedings.*

*Columbia University, New York, New York.
†Princeton Plasma Physics Laboratory, Princeton, New Jersey.
‡Lawrence Livermore National Laboratory, Livermore, California.
ΔChalmers University of Technology, Göteborg, Sweden.

Work supported by
the U.S. Department of Energy
under DE-FG02-89ER53297, DE-AC02-76CH03073,
DE-FG03-95ER54309, DE-FC02-04ER54698, and W-7405-ENG-48

GENERAL ATOMICS PROJECT 30200
OCTOBER 2004

Measurement of Resistive Wall Mode Stability in Rotating High Beta Plasmas

H. Reimerdes,[1] J. Bialek,[1] M.S. Chance,[2] M.S. Chu,[3] A.M. Garofalo,[1] P. Gohil,[3] G.L. Jackson,[3] R.J. Jayakumar,[4] T.H. Jensen,[3] R.J. La Haye,[3] Y.Q. Liu,[5] J.E. Menard,[2] G.A. Navratil,[1] M. Okabayashi,[2] J.T. Scoville,[3] E.J. Strait[3] and H. Takahashi[2]

[1]Columbia University, New York, New York, USA
[2]Princeton Plasma Physics Laboratory, Princeton, New Jersey, USA
[3]General Atomics, San Diego, California, USA
[4]Lawrence Livermore National Laboratory, Livermore, California, USA
[5]Chalmers University of Technology, Göteborg, Sweden

e-mail contact of main author: reimerdes@fusion.gat.com

Abstract. Toroidal plasma rotation in the order of a few percent of the Alfvén velocity can stabilize the resistive wall mode and extend the operating regime of tokamaks from the conventional, ideal MHD no-wall limit up to the ideal MHD ideal wall limit. The stabilizing effect has been measured passively by measuring the critical plasma rotation required for stability and actively by probing the plasma with externally applied resonant magnetic fields. These measurements are compared to predictions of rotational stabilization of the sound wave damping and of the kinetic damping model using the MARS code.

1. Introduction

Rapid toroidal plasma rotation past a conducting wall affects the stability of high-β plasmas. In neutral beam heated DIII-D plasmas, a rotation frequency in the order of a few percent of the inverse Alfvén time is sufficient to stabilize the resistive-wall mode (RWM) up to the ideal MHD ideal wall limit [1]. The stabilization of the RWM could increase the operating regime of tokamaks from the conventional, no-wall stability limit, $\beta_{\text{no-wall}}$, up to the ideal wall limit, $\beta_{\text{ideal-wall}}$, and hence allow for smaller and more efficient fusion reactors. Operation above $\beta_{\text{no-wall}}$ is particularly important in advanced tokamak (AT) scenarios, which aim at steady-state operation with a large fraction of pressure driven bootstrap current.

Dissipation is thought to be the mechanism responsible for RWM stabilization by plasma rotation [2], but the form of the dissipation has been under debate for the last decade. In the "sound wave damping" model the perturbation of the plasma rotation caused by the RWM couples to sound waves, which are then subject to ion Landau damping. Alternatively, the electromagnetic perturbation can be kinetically damped through the Landau damping process [3]. This is referred to as "kinetic damping". A reliable extrapolation of the stabilizing effect of plasma rotation and, in particular, of the rotation required for stable operation, Ω_{crit}, to a future experiment requires a complete understanding of the underlying dissipative process.

To test the proposed damping models, the stability of high-β plasmas has been probed passively by measuring Ω_{crit} and actively by applying resonant fields with non-axisymmetric control coils. In the presence of a weakly damped mode, such as the RWM in a rapidly rotating high-β plasma, the plasma amplifies the resonant component of the applied field, a phenomenon referred to as resonant field amplification (RFA) [4]. The source of the applied field can be currents in non-axisymmetric control coils as well as the resonant component of the intrinsic error field. The amplification of an uncorrected intrinsic error results in an enhanced drag and can deteriorate the momentum confinement at high β. If measured, RFA reveals information about the (negative) growth rate and toroidal mode rotation frequency of the stable RWM. The comparison of the stability measurements with numerical calculations using the MARS code [5] directly tests the proposed dissipation mechanisms.

2. Active Measurement of RWM Stability

In DIII-D the RWM stability can be probed with two sets of non-axisymmetric coils: the C coil, located on the outboard midplane outside the vacuum vessel and the I coil, located above and below the midplane inside the vacuum vessel, Fig. 1(a). The individual coils can

be phased to generate pulsed or rotating magnetic fields that overlap with long wavelength, low-n external kink modes, which are generally the most unstable global modes. The perturbed field B_s is detected with several toroidal arrays of poloidal and radial field sensors, Fig. 1(a), where the index s denotes the sensor array. Quantities that exhibit the toroidal symmetry of the mode are represented by a complex number such that $f(t,\varphi) = \Re\left(F(t)\cdot e^{-in\varphi}\right)$ with a positive φ pointing in the direction of the plasma rotation. The plasma response is obtained by subtracting the externally applied field, $B_s^{plas} = B_s - B_s^{ext}$, where B_s^{ext} has been measured in vacuum experiments and includes the contribution of the corresponding eddy currents. The RFA amplitude is defined as the ratio of plasma response and vacuum field,

$$A_{RFA,s} = B_s^{plas} / B_s^{ext} \quad , \tag{1}$$

and strongly depends on the sensor location and the geometry of the applied field. Using the complex notation the phase of $A_{RFA,s}$ describes the toroidal phase shift of the plasma response with respect to the externally applied field.

Experiments using n = 1 C coil pulses have shown that the plasma response observed at high β has the same structure as the unstable RWM [4]. Fig. 1(b) shows n = 1 pulses with the I coil. A toroidal phase difference of the n = 1 field of the upper and lower I coil arrays of 240° maximizes the overlap with the RWM structure at the wall. The plasma response is proportional to I_c, Fig. 1(c,d). The linearity holds for different sensors albeit with a different ratio, Fig. 1(e,f). The linear dependence fails at large perturbation amplitude, where plasma rotation and β are degraded and the stability properties of the plasma change. The stability is generally probed with a small amplitude perturbation $B_s^{ext}/B_0 \approx 10^{-4} - 10^{-3}$, where the linearity of the plasma response is a good assumption.

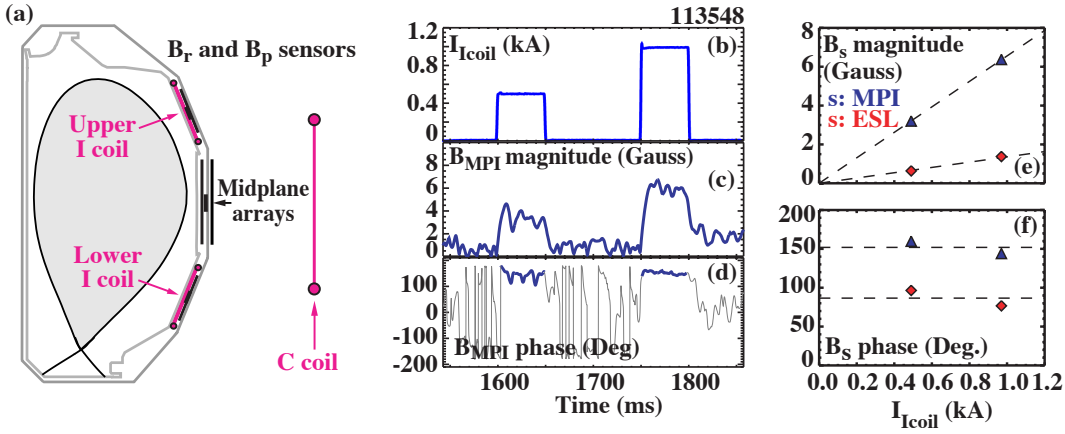

Fig. 1. (a) Poloidal cross-section of DIII-D plasma with the location of I and C coils and various magnetic sensors. (b) Resonant n = 1 I coil pulses, (c) magnitude and (d) toroidal phase of the resulting n = 1 plasma response measured with poloidal field probes on the midplane (MPI). (e) The magnitude of the plasma response measured with MPI sensors and saddle loops on the midplane (ESL) increases linearly with the applied current while (f) its toroidal phase remains constant.

2.1. Single Mode Description of RFA

The simplest approach to describe the interaction between the plasma and externally applied fields is a single mode model [6,7]. While the models differ in their dispersion relation for the RWM growth rate in the absence of external currents, γ_0, they yield the same evolution equation for the resonant component of the perturbed radial field at the wall [8,9],

$$\tau_w \frac{dB_s}{dt} - \gamma_0 \tau_w B_s = M_{sc}^* I_c \quad . \tag{2}$$

In the complex notation, $\Re(\gamma_0)$ is the growth rate and $\Im(\gamma_0)$ the toroidal rotation frequency of the mode. The effective mutual inductance M_{sc}^{*} describes the direct coupling between the control coil current I_c and the resonant component of the externally applied field at the wall. It depends on the geometry of the applied field and the RWM structure. The characteristic wall time τ_w is defined as the decay time for wall currents induced by the mode. In the absence of plasma, $\gamma_0 = -1/\tau_w$. In slab geometry τ_w for a mode with a wavenumber k is,

$$\tau_w = (\Delta\mu_0)/(2k\eta) \quad , \tag{3}$$

where Δ and η are the thickness and resistivity of the vessel respectively. Using a typical k of the n = 1 RWM at the outboard midplane in DIII-D, Eq. (3) yields τ_w of 2.4 ms [4]. An independent estimate for τ_w is obtained from the attenuation of an externally applied rotating magnetic field, B_s^{ext}, which has a similar structure as the RWM, without a plasma. A comparison of the vacuum measurement of $B_s^{ext}(\omega_{ext})$ and the predicted frequency dependence $B_s^{ext}(\omega_{ext}) = M_{sc}I_c/(1+i\omega_{ext}\tau_w)$, obtained from Eq. (2), yields τ_w of 2.5 ms. Here, M_{sc} is the total mutual inductance between I_c and the field measured with the sensor s.

2.2. Dynamic Response to a Pulsed Resonant Field

The plasma can be probed with a pulsed magnetic field. Once the eddy currents have decayed all parameters are constant (d/dt = 0) and Eq. (2) yields,

$$A_{RFA,s} = c_s \cdot (1+\gamma_0\tau_w)/(-\gamma_0\tau_w) \quad , \tag{4}$$

where $c_s = M_{sc}^{*}/M_{sc}$ is the ratio of the resonant component of the externally applied field and the total externally applied field detected with the sensors s and arises from the different structure of the magnetic fields in the numerator and denominator of the definition of $A_{RFA,s}$, Eq. (1). Once I_c is switched off, the perturbation amplitude evolves according to,

$$B_s(t) = B_s(0)\cdot e^{\gamma_0 t} \quad , \tag{5}$$

with $\Re(\gamma_0) < 0$, if the mode is stable. DIII-D experiments, where n = 1 C coil pulses are applied at various values of β, yield a measurement of the magnitude and phase of $A_{RFA,s}$ during the pulses. RFA is observed when β exceeds the no-wall limit, Fig. 2(a), where the phase increases continuously with β, Fig. 2(b). The same experiment also yields a measurement of the decay of the perturbation $B_s(t)$ after the pulse is switched off [8]. By inverting Eq. (4) a value for γ_0 can be calculated from each measurement of $A_{RFA,s}$,

$$\gamma_0\tau_w = \left[1-(A_{RFA,s}/c_s)\right]^{-1} \quad . \tag{6}$$

The calculated value of γ_0 is compared to the measured decay of the perturbation after the pulse. Here, only the damping rate, i.e. $\Re(\gamma_0)$, is extracted from the dynamic response. By fitting the geometry parameter c_s, reasonable agreement between these two independent measurements of $\Re(\gamma_0)$ is obtained, Fig. 2(c), showing the applicability of the model [8].

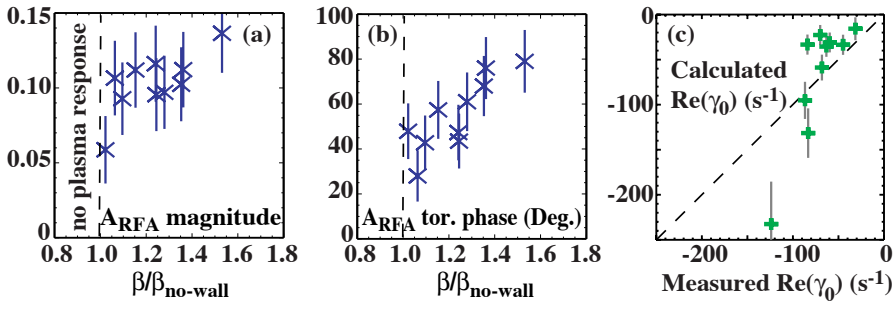

Fig. 2. RFA magnitude (a) and toroidal phase (b) for n = 1 pulses with the C coil yield a value of the (negative) RWM growth rate (c) which is compared to the measured decay rate after the pulse is switched off.

2.3. RFA Spectrum

The experiment is generalized by applying an external field as a traveling wave with various angular frequencies ω_{ext}. After an initial transient phase all quantities oscillate with the externally imposed frequency and Eq. (2) yields the RFA spectrum,

$$A_{RFA,s}(\omega_{ext}) = c_s \cdot (1+\gamma_0\tau_w)/(i\,\omega_{ext}\,\tau_w - \gamma_0\tau_w) \quad . \tag{7}$$

According to Eq. (7) the RFA peaks when ω_{ext} matches $\Im(\gamma_0)$. The maximum RFA magnitude increases as the plasma approaches marginal stability and diverges at marginal stability. In DIII-D experiments the individual I coils are phased to generate a rotating n = 1 field [10]. The perturbed field is extracted as the Fourier coefficient at ω_{ext}. The frequency is varied in identically prepared discharges. The RFA spectrum, measured at two values of β, is compared in Fig. 3 to the single mode prediction, Eq. (7). The RFA is largest for an externally applied field rotating slowly, $\omega_{ext} < 1/\tau_w$, in the direction of plasma rotation. The resonance becomes sharper as β increases, consistent with weaker damping. Fitting two free complex parameters γ_0 and c_s leads to good agreement at both values of β. The values of c_s resulting from both fits are equal (within 10%), consistent with a factor that depends only on the geometry of the sensors and the mode. The good agreement between the measured spectrum and the fit confirms that the interaction between the RWM and externally applied magnetic fields is well described by a single mode model. Consequently, the fit parameter yields an absolute measurement of γ_0. This is the extension of the technique of "active MHD spectroscopy", previously applied at frequencies above 10 kHz [11], to frequencies of a few Hertz.

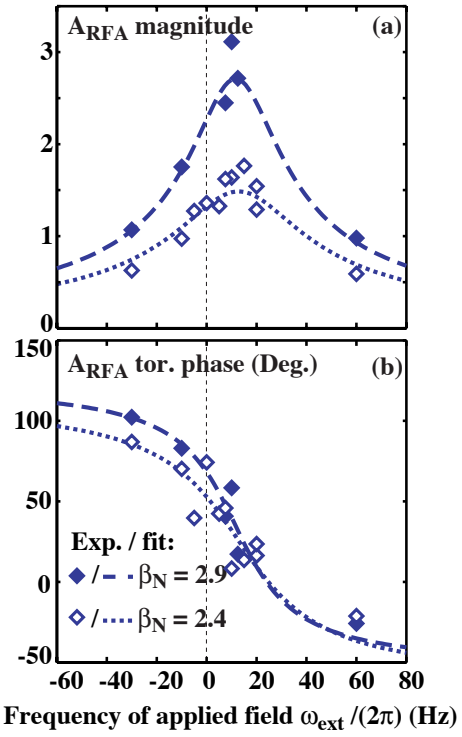

Fig. 3. Measured spectrum of the (a) magnitude and (b) toroidal phase of the RFA at two values of β_N using saddle loops in the midplane (ESL) and fit to single-mode model, Eq. (7).

2.4. Continuous Measurement

Once the coupling parameter c_s is known, the measurement of the RFA at a single frequency is sufficient to determine the RWM stability allowing for a continuous measurement of ideal MHD stability in a single discharge,

$$\gamma_0\tau_w = (i\omega_{ext}\tau_w A_{RFA,s}/c_s - 1)/(A_{RFA,s}/c_s + 1) \quad . \tag{8}$$

An example of such a measurement is shown in Fig. 4 in which a low-amplitude external field with $\omega_{ext}/(2\pi) = 20$ Hz is applied during a discharge as β is increased up to an RWM onset. Real and imaginary parts of γ_0 are derived from the measurement of $A_{RFA,s}$ using the value of c_s obtained from the fit of the complete RFA spectrum shown in Fig. 3. The measured growth rate increases as β exceeds the no-wall limit. The mode rotation frequency remains small.

3. Critical Plasma Rotation Frequency

The most important parameter is the critical plasma rotation frequency Ω_{crit}, which is required for RWM stability. It has been measured in neutral beam heated DIII-D plasmas and is compared to MARS predictions for sound wave and kinetic damping. The sound wave damping is implemented with an adjustable parameter $\kappa_{||}$, which describes the effect of

toroidicity and shaping, with $\kappa_{||} = 1$ being the limit of a large aspect ratio cylinder. In a realistic geometry $\kappa_{||}$ is estimated to be approximately 0.5. The kinetic damping model has no free parameters. In order to compare the stabilizing effect of plasma rotation in different scenarios a normalized gain of β above the no-wall limit, $C_\beta = (\beta - \beta_{no\text{-}wall})/(\beta_{ideal\text{-}wall} - \beta_{no\text{-}wall})$, is used to characterize the RWM strength in the absence of rotation. The RWM can become unstable for $C_\beta > 0$ and is replaced by the plasma mode as the dominant global mode at $C_\beta \approx 1$.

3.1. Measurement of the Critical Plasma Rotation Frequency

A systematic measurement of Ω_{crit} has been carried out in plasmas where weak shaping, similar to the shape shown in Fig. 1(a), and a low internal inductance l_i lead to a low β-limit guaranteeing that the n = 1 RWM is the relevant stability limit [12]. Ideal MHD calculations using the GATO code [13] show that $\beta_{N,no\text{-}wall} = 2.4\, l_i$ is a good approximation of the no-wall limit. Due to the broad current profile, with l_i typically being 0.67, the plasma greatly benefits from wall stabilization with a calculated $\beta_{N,ideal\text{-}wall} \approx 3.2$ corresponding to 4.8 l_i. In these discharges β_N exceeds $\beta_{N,no\text{-}wall}$, Fig. 5(a). An incomplete correction of the error field leads to a decrease of the plasma rotation, which is measured with a CER diagnostic using C^{VI+}, Fig. 5(b). Once the rotation is no longer sufficient to stabilize the mode, the RWM grows leading to a much faster decrease of the rotation and a β-collapse. The RWM onset marks Ω_{crit}. It is found that Ω_{crit}, measured at the q = 2, scales like $\Omega_{crit}\,\tau_A \approx 0.02$ [14], where the local Alfvén time is defined as $\tau_A = R_0(\mu_0\rho)^{1/2}/B_0$ with R_0 being the major radius, B_0 the magnetic field on axis and ρ the local mass density. The Ω_{crit} measurement is carried out for various values of β ranging from $\beta_{N,no\text{-}wall}$, corresponding to $C_\beta = 0$, to $\beta_{N,ideal\text{-}wall}$, corresponding to $C_\beta = 1$. The safety factor at the RWM onset is typically $q_{95} = 3.6$. While Ω_{crit} shows no significant dependence on C_β the standard deviation at each value of C_β is large, Fig 5(d). The RWM onsets at $C_\beta < 0$ reflect the uncertainty of the no-wall limit.

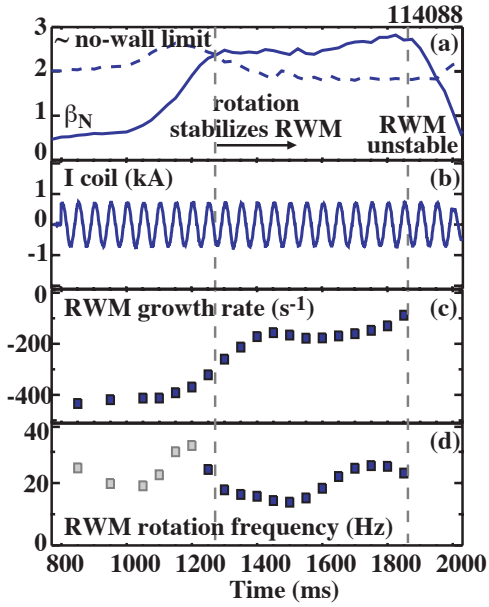

Fig. 4. (a) β_N is increased above the no-wall limit. (b) The I coil generates a rotating n = 1 field with $\omega_{ext}/(2\pi) = 20$ Hz. (c) RWM growth rate and (d) mode rotation frequency are obtained from the RFA measured at ω_{ext} with midplane saddle loops, Eq. (8).

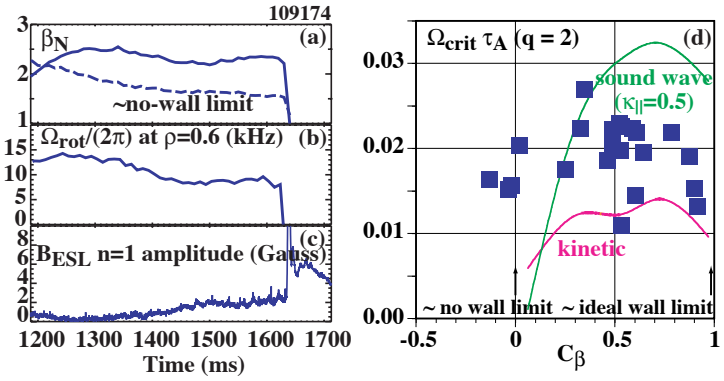

Fig. 5. (a) When β_N exceeds the no-wall limit, (b) the toroidal plasma rotation decreases until the onset of an n = 1 RWM (c) seen with saddle loops in the midplane. (d) Measurements of $\Omega_{crit}\tau_A$ at q = 2 are compared with MARS predictions for sound wave damping ($\kappa_{||} = 0.5$) and kinetic damping.

3.2. Comparison with MARS

The critical rotation frequency has been calculated for a typical low-l_i equilibrium. The experimental pressure profile is scaled from the no-wall to the ideal wall limit keeping the

total plasma current constant. At each pressure the measured rotation profile is scaled until marginal stability is found. The calculated critical rotation frequency at q = 2 using the sound wave damping model with $\kappa_{||} = 0.5$ and the kinetic damping model are compared with the measurements, Fig 5(d) [11]. While sound wave damping underestimates Ω_{crit} frequency for C_β from 0 to 0.2, it overestimates it for C_β greater than 0.4. Kinetic damping predicts a weak dependence of Ω_{crit} on C_β but underestimates the magnitude of Ω_{crit} by approximately 40%.

4. RWM Damping Rate and Mode Rotation Frequency

Active measurements reveal information about the magnitude of the damping, i.e. negative growth rate, and the mode rotation frequency without the RWM becoming unstable. The measurements are carried out with the two methods described above in scenarios that differ in l_i. The measurements of γ_0 are compared to MARS predictions.

4.1. Measurement of the RWM damping rate and mode rotation frequency

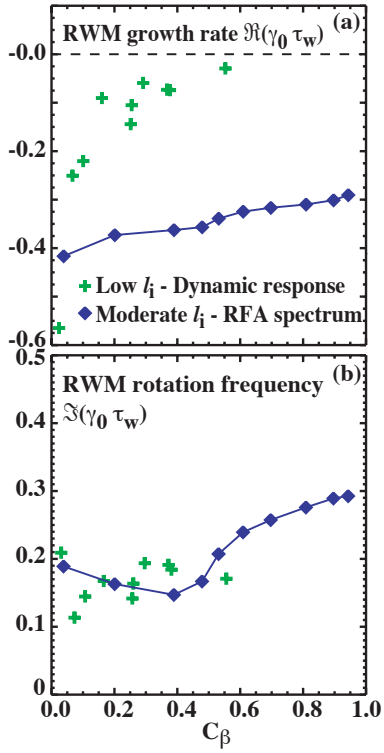

Fig. 6. RWM growth rate (a) and mode rotation frequency (b) obtained from the dynamic response to C coil pulses in low-l_i plasmas (crosses) and the RFA spectrum using rotating I coil fields in moderate-l_i plasmas (diamonds).

The active measurement, using the dynamic response to pulses, is applied in the same low-l_i scenario used for the measurement of Ω_{crit}, but with optimized error field correction to sustain the plasma rotation at $\Omega_{rot} \approx 0.02 \cdot \tau_A^{-1} > \Omega_{crit}$. The n = 1 pulses are applied with the C coil while β_N is increased. The plasma response is measured by the midplane saddle loops and poloidal field probes. The values of γ_0 are calculated as a best fit to the measured RFA amplitude and phase and decay after the pulse is switched off and are shown as a function of C_β, Fig 6(a). The sudden rise of the plasma response once C_β exceeds 0, Fig 2(a), is reflected in an equally sudden decrease in the RWM damping rate. The damping rate continuously decreases and approaches marginal stability at $C_\beta \approx 0.6$. The mode rotation frequency is found to be a fraction of the inverse wall time with little dependence on C_β, Fig 6(b).

The active measurement using the RFA spectrum is applied in a similar plasma shape, but at a higher l_i of typically 0.85. Ideal MHD calculation using the DCON code [15] have shown that while $\beta_{N,no\text{-}wall} = 2.4\, l_i$ still holds, the potential gain through wall stabilization decreases relative to l_i. The ideal wall limit for β_N is found to be approximately 3.2 corresponding to 3.8 l_i. The rotating n = 1 field is applied with the I coil while β_N is increased, Fig. 7(a). During the measurement q_{95} decreases continuously from 4.4 to 3.8. At the same time the plasma rotation of $\Omega_{rot}\tau_A \approx 0.02$ at q = 2 is sustained using optimum error field correction. The plasma rotation is well above the critical rotation of $\Omega_{crit}\tau_A \approx 0.01$ typically observed in these moderate-l_i discharges. The n = 1 plasma response is measured with the midplane saddle loops and its magnitude and phase with respect to the applied current extracted using a Fourier transform of 200 ms intervals, Fig. 7(b,c). The experiment is then repeated in identically prepared discharges with different frequencies, scanning $\omega_{ext}/(2\pi)$ from –20 to +40 Hz. For all values of ω_{ext} the plasma response increases significantly once β_N exceeds the no-wall limit. The values of γ_0 are calculated from the measured RFA spectrum. The growth rate is seen to increase towards marginal stability as β_N is increased, Fig 6(a). The measurements indicate that the RWM is more damped in the moderate-l_i plasma than in the low-l_i plasma. This is consistent with the significantly lower critical rotation observed in the moderate-l_i plasmas. The uncertainty in the coupling factors c_s used for the C and I coils

could, however, lead to a systematic uncertainty of the γ_0 measurement. The mode rotation frequency is low, on the order of a fraction of the inverse wall time, which is in good agreement with the C coil experiment, and increases with increasing β_N, Fig 6(b).

4.2. Comparison with MARS

The growth rate and mode rotation frequency have been calculated for a typical moderate- l_i equilibrium using the sound wave damping model with $\kappa_{||} = 0.5$ and the kinetic damping model. The experimental pressure profile is scaled from the no-wall to the ideal wall limit keeping the q-profile constant. At each pressure the measured rotation profile is varied and the RWM growth rate γ_0 calculated, Fig 8. It is found that for both damping models only $\Omega_{rot}\tau_A \approx 0.005$ at $q = 2$ is sufficient to stabilize the RWM up to values of C_β close to 1, showing that both damping models predict significantly stronger damping for this plasma than for the low-l_i plasma. The main difference in the moderate-l_i equilibrium is the higher edge q used in the stability calculations with the q = 5 and 6 surface being present. The MARS predictions are compared to the measured RWM growth rate and mode rotation frequencies, Fig. 8. The calculations reproduce the trend of a reduction of the damping and an increase of the mode rotation frequency with increasing C_β. Both damping models overestimate the damping. They also tend to overestimate the mode rotation frequency.

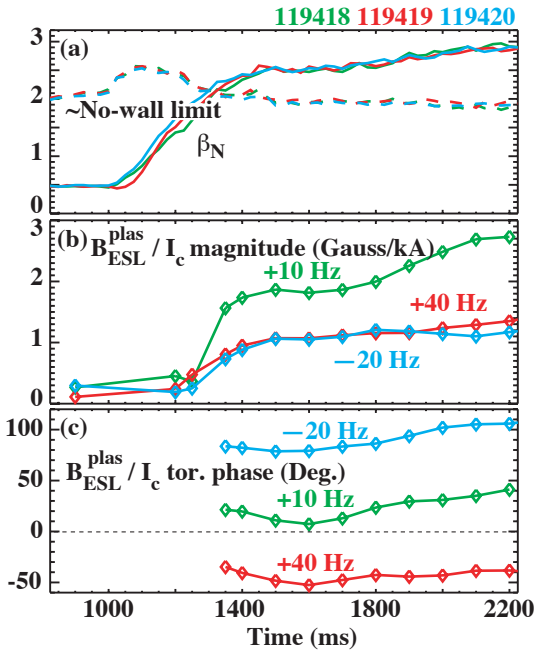

Fig. 7. (a) β_N and estimated no-wall limit. (b) Magnitude and (c) phase of the n = 1 plasma response at the applied frequency normalized on the applied current.

5. Predictions for DIII-D Advanced Tokamak Scenarios

MARS has also been used to predict the stabilizing effect of plasma rotation in DIII-D AT scenarios. One goal of the AT is the optimization of the current profile with respect to transport, bootstrap current alignment and MHD stability. In order to address the potential of rotational stabilization a set of equilibria with the same edge safety factor $q_a = 7.2$, but different values of q_{min} has been analyzed, Fig. 9. Here, sound wave damping with $\kappa_{||} = 0.28$ and kinetic damping are used. While the existence of the q = 3/2 surface has little effect on the rotational stabilization, there is a significant increase of $\Omega_{crit}\tau_A$ (now evaluated at the q = 3 surface) when q_{min} is raised above 2. The large

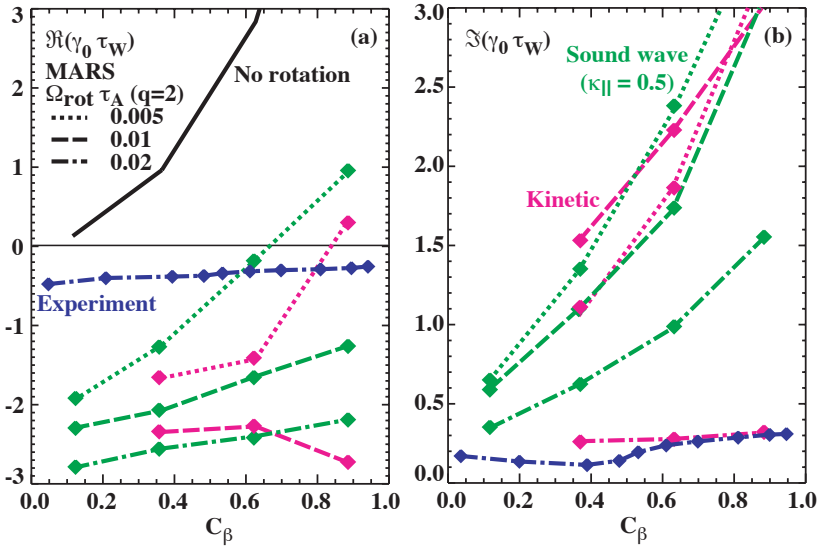

Fig. 8. The RWM growth rate (a) and mode rotation frequency (b) measured with rotating I coil fields in the moderate-l_i scenario are compared to MARS predictions for sound wave damping ($\kappa_{||} = 0.5$) and kinetic damping with various values of plasma rotation Ω_{rot}.

contribution of the q = 2 surface to rotational stabilization is also seen in the kinetic damping model, albeit at a lower value of $\Omega_{crit}\tau_A$. While the high q_{min} current profile is attractive with respect to tearing mode stability, these MARS calculations suggest that it might require feedback stabilization of the RWM.

6. Summary

The stabilizing effect of rotation on the n = 1 ideal kink mode is observed in DIII-D and allows for operation above the conventional, no-wall stability limit up to the ideal wall limit. The stabilizing effect is quantified using the passive measurement of Ω_{crit} as well as active measurements probing the plasma with externally applied fields. Once the plasma exceeds the no-wall stability limit it responds to applied resonant fields. The time evolution as well as frequency dependence of the plasma response is well described by a single mode model, which in turn can be used to obtain a measurement of the growth rate and mode rotation frequency of a marginally stable RWM. Such a measurement carried out at a single frequency looks promising as a real-time indication of the approach to the stability limit and can be an important input for profile control in an AT. The passive and active measurements of RWM stability in DIII-D are compared to MARS modeling of rotational stabilization. The experiment and the modeling, both, show that the plasma rotation has a stronger stabilizing effect on a moderate-l_i plasma than on a low-l_i plasma with lower q_{95}, indicating the importance of resonant surfaces for the stabilization mechanism. An analysis of Ω_{crit} in the low-l_i target suggests that sound wave damping underestimates the stabilizing effect while kinetic damping overestimates the stabilizing effect of rotation. The measurements of the damping rate and mode rotation frequency of the stable RWM in moderate-l_i plasmas indicate that both models overestimate the damping of the RWM. Progress is being made in the experimental and modeling effort towards a quantitative test of the proposed damping models.

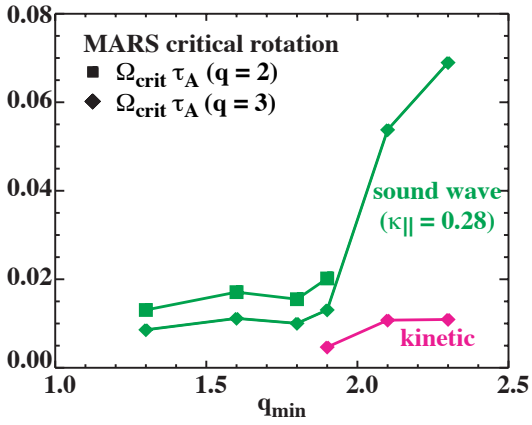

Fig. 9. MARS calculations of $\Omega_{crit}\tau_A$ at the q = 2 and q = 3 surface in an DIII-D advanced tokamak scenario depend on q_{min}. Sound wave damping ($\kappa_{||} = 0.28$) and kinetic damping predict a significant increase of $\Omega_{crit}\tau_A$ when q_{min} is raised above 2.

Acknowledgment

Work supported by U.S. Department of Energy under DE-FG02-89ER53297, DE-AC02-76CH03073, and DE-FC02-04ER54698.

References

[1] GAROFALO, A.M., *et al.,* Phys. Rev. Lett. **89** (2002) 235001.
[2] BONDESON, A. and WARD, D.J., Phys. Rev. Lett. **72** (1994) 2709.
[3] BONDESON, A. and CHU, M.S., Phys. Plasmas **3**, (1996) 3013.
[4] BOOZER, A.H., Phys. Rev. Lett. **86** (2001) 1176.
[5] LIU, Y.Q., *et al.,* Phys. Plasmas **7** (2000) 3681.
[6] GAROFALO, A.M., JENSEN, T.H., and STRAIT, E.J., Phys. Plasmas **9**, 4573 (2002).
[7] OKABAYASHI, M., et al Plasma Phys. Control. Fusion **44** (2002) B339.
[8] GAROFALO, A.M., JENSEN, T.H., and STRAIT, E.J., Phys. Plasmas **10** (2003) 4776.
[9] CHU, M.S., *et al.,* Nucl. Fusion **43** (2003) 196.
[10] REIMERDES, H., *et al*, Phys. Rev. Lett. **93** (2004) 135002.
[11] FASOLI, A., *et al.,* Phys. Rev Lett. **75** (1995) 645.
[12] GAROFALO, A.M., *et al.,* Phys. Rev. Lett. **82** (1999) 3811.
[13] BERNARD, L.C., HELTON, F.J., and MOORE, R.W., Comput. Phys. Commun. **21** (1981) 377.
[14] LA HAYE, R.J., *et al.,* accepted for publication in Nucl. Fusion.
[15] GLASSER, A. and CHANCE, M.S., Am. Phys. Soc. **42** (1997) 1848.